Remarkable Uptake of CO2 and CH4 by Graphene-Like Borocarbonitrides, BxCyNz

ARTICLE *in* CHEMSUSCHEM · NOVEMBER 2011

Impact Factor: 7.66 · DOI: 10.1002/cssc.201100197 · Source: PubMed

CHEMSUSCHEM

DOI: 10.1002/cssc.201100197

Remarkable Uptake of CO_2 and CH_4 by Graphene-Like Borocarbonitrides, $B_xC_yN_z$

Nitesh Kumar, K. S. Subrahmanyam, Piyush Chaturbedy, Kalyan Raidongia, Achutharao Govindaraj, Kailash P. S. S. Hembram, Abhishek K. Mishra, Umesh V. Waghmare, and C. N. R. Rao*[a]

The surface areas and uptake of CO_2 and CH_4 by four graphene samples are measured and compared with activated charcoal. The surface areas are in the range of 5–640 $m^2 g^{-1}$, whereas the CO_2 and CH_4 uptake values are in the range of 18–45 wt% (at 195 K, 0.1 MPa) and 0–2.8 wt% (at 273 K, 5 MPa), respectively. The CO_2 and CH_4 uptake values of the graphene samples vary linearly with the surface area. In contrast, graphene-like $B_xC_yN_z$ samples with compositions close to BC_2N exhibit surface areas in the range of 1500–1990 $m^2 g^{-1}$ and CO_2 and CH_4 uptake values in the ranges 97–128 wt% (at 195 K, 0.1 MPa) and 7.5–17.3 wt%, respectively. The uptake of these gases varies exponentially with the surface area of the $B_xC_yZ_n$ samples, and the uptake of CH_4 varies proportionally with that of CO_2. The uptake of CO_2 for the best BC_2N sample is 64 wt% at 298 K. The large uptake of both CO_2 and CH_4 gases by BC_2N betters the performance of graphenes and activated charcoal. First-principles calculations show that the adsorption of CO_2 and CH_4 is more favored on BCN samples compared to graphene.

Introduction

Methane and carbon dioxide are the two main gases responsible for global warming and other harmful effects. Therefore, it is important to explore possibilities to minimize and eliminate the presence of these gases in the atmosphere. In the case of CO_2, methods have been proposed to capture it in various materials and utilize it in chemical reactions.[1] Removing low concentrations of CO_2 from air is rather difficult, however, removal of CO_2 from flue gases is more practical.[2,3] For this purpose, CO_2 has been dissolved in solvents, such as organic amines.[4–14] This method generally suffers from difficulties related to the regeneration of the solvents by heating.[15] Solid sorbents would be more economical and metal-organic frameworks (MOFs) and other solids have been investigated for this purpose.[16–25] Activated carbons have shown good potential to adsorb CO_2.[26,27] A considerable amount of work on the removal of CO_2 has been reported, whereas elimination of CH_4 from the atmosphere has received somewhat less attention. Removal of CH_4 by sorbents is generally much less effective than removal of CO_2. MOFs have been reported to adsorb reasonable volumes of CH_4.[28–34] Thus, Ma et al.[30] reported high CH_4 adsorption (230 *v/v* at 298 K and 3.5 MPa) using PCN-14, which is an anthracene-derived MOF. Activated charcoal and carbon fiber display reasonably good CH_4 adsorbance.[35]

We considered it worthwhile to explore the adsorption of CO_2 and CH_4 on few-layer graphene samples prepared by using a variety of methods and compare the results with those of inorganic graphene analogues containing boron, carbon, and nitrogen, $B_xC_yN_z$. Interest in the latter arose from a recent observation that a graphene-like borocarbonitride (BCN) sample exhibited a high surface area and good adsorption for CO_2 at low temperatures.[36] Herein, we report our experimental results on the uptake of CO_2 and CH_4 by four graphene samples and by five graphene-like $B_xC_yN_z$ samples with compositions close to BC_2N. We found extraordinary uptake of both CO_2 and CH_4 by some of the $B_xC_yN_z$ samples, even at room temperature. We have employed first-principles calculations to understand why $B_xC_yN_z$ samples possess such remarkable adsorption properties.

Results and discussion

Four graphene samples, EG, HG, RGO, and SGO, were examined; the sample EG was prepared by thermal exfoliation of graphitic oxide,[37–39] whereas HG was prepared by evaporation of graphite in hydrogen,[40] SGO by ultrasonication of graphitic oxide, and RGO by reduction of SGO.[41] Typical TEM and AFM images of EG and HG are shown in Figure 1. AFM measurements of the four graphene samples show that SGO has the least number of layers (ca. 1–2), EG and RGO have 6–7 layers and HG consists of 2–3 layers; the TEM image of HG also clearly shows the presence of 2–3 layers. The Brunauer–Emmett–Teller (BET) surface area of the graphene samples (SGO, HG, EG, and RGO) were measured, along with that of a sample of

[a] N. Kumar, K. S. Subrahmanyam, P. Chaturbedy, Dr. K. Raidongia, Dr. A. Govindaraj, Dr. K. P. S. S. Hembram, Dr. A. K. Mishra, Prof. U. V. Waghmare, Prof. C. N. R. Rao
Chemistry and Physics of Materials Unit
CSIR Centre of Excellence in Chemistry and
International Centre for Materials Science
Theoretical Sciences Unit, Jawaharlal Nehru
Centre for Advanced Scientific Research
Jakkur, Bangalore, 560064 (India)
E-mail: cnrrao@jncasr.ac.in

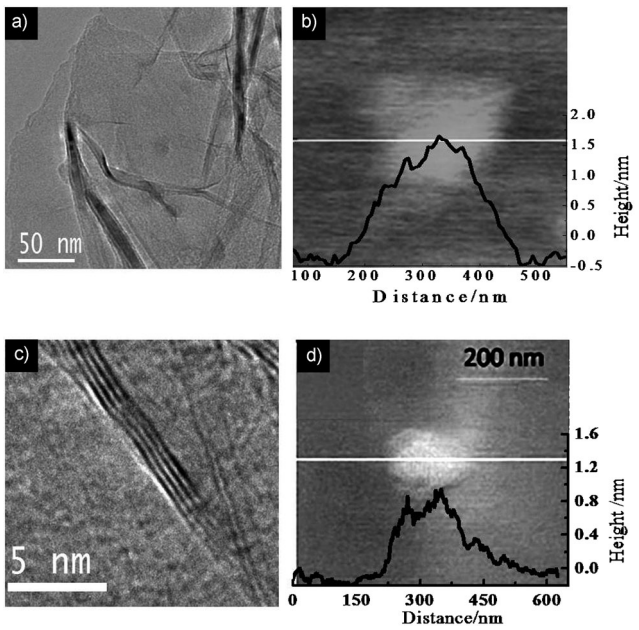

Figure 1. TEM images of a) EG and c) HG; AFM images of b) EG and d) HG.

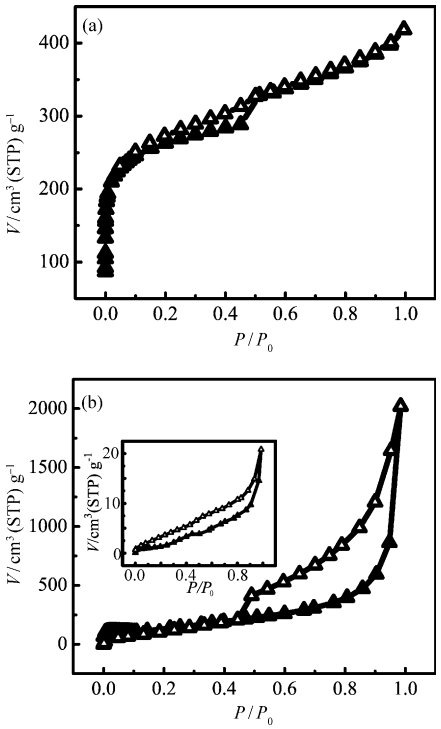

Figure 2. N_2-adsorption (▲) and -desorption (△) isotherms at 77 K and 0.1 MPa of a) activated charcoal and b) EG; SGO shown in inset.

activated charcoal (SD Fine Chem. Ltd). Typical N_2 adsorption data recorded at 77 K and 0.1 MPa are shown in Figure 2. The surface areas of activated charcoal and graphene samples vary between 5–1250 $m^2 g^{-1}$. Within the graphene samples, EG shows the highest surface area of 640 $m^2 g^{-1}$ and SGO the lowest value of 5 $m^2 g^{-1}$; activated charcoal has a surface area of 1250 $m^2 g^{-1}$. The surface area values and the number of graphene layers for the graphene samples and activated charcoal are listed in Table 1.

Uptake of CO_2 by the graphene samples and activated charcoal was measured at 195 K and 0.1 MPa. Typical CO_2 adsorption data are shown in Figure 3. The uptake values range between 5–45 wt% for the graphene samples, with EG exhibiting the highest uptake. Activated charcoal shows 64 wt% uptake of CO_2 at 195 K and 0.1 MPa; the uptake of CO_2 by EG at 298 K and 5 MPa was 51 wt%. Adsorption of CH_4 on the graphene samples and activated charcoal was measured at 273 and 298 K. Typical adsorption data are shown in Figure 4. The uptake of CH_4 by activated charcoal is 7 and 6 wt% at 273 and 298 K, respectively. The CH_4 uptake of the graphene samples varies between 0 and 3 wt%. The uptake values of both CH_4 and CO_2 by the graphene samples are listed in Table 1 along with the data for activated charcoal. The uptake of CO_2 and CH_4 follows similar trends; in Figure 5a, the uptake of CO_2 and CH_4 are plotted against the surface area. The uptake values of CH_4 and CO_2 vary linearly with the surface area. A plot of the CH_4 versus CO_2 uptake is almost linear (Figure 5b). EG and RGO, which have relatively high CO_2 and CH_4 uptakes, contain oxygen functionalities on the surface. Interestingly, the surface is clean with negligible oxygen functionality in the case of HG, which shows little or no uptake of these gases.

Table 1. Layer and gas adsorption data of activated charcoal, EG, RGO, HG, and SGO.

Sample	Number of layers	Surface area [$m^2 g^{-1}$]	CO_2 adsorption[a] [wt%]	CH_4 adsorption[b] [wt%] 298 K	273 K
Activated charcoal	∞	1250	64	6.0	7.0
EG	6	640	45[c]	2.4	2.8
RGO	6	373	27	1.7	2.5
HG	3	240	5	0.0	–
SGO	1	5	18	0.4	–

[a] At 195 K and 0.1 MPa. [b] At 5 MPa. [c] Uptake at 298 K and 5 MPawas 51 wt%.

The five $B_xC_yN_z$ samples possess graphene-like layered structures. The reactions involved in the formation of $B_xC_yN_z$ samples are shown below. The sample composition depends on the relative proportion of carbon, but in practice, Equations (3) and (4) may occur simultaneously to different extents. Equation (4) is more predominant than Equation (3) under the conditions of the our experiments.

$$2\,H_3BO_3 \xrightarrow{\Delta} B_2O_3 + 3\,H_2O \quad (1)$$

$$CO(NH_2)_2 \xrightarrow{\Delta} NH_3 + HNCO \quad (2)$$

$$B_2O_3 + 2\,NH_3 + 2\,C \xrightarrow{\Delta} 2\,BCN + 3\,H_2O \quad (3)$$

$$B_2O_3 + 2\,NH_3 + 4\,C \xrightarrow{\Delta} 2\,BC_2N + 3\,H_2O \quad (4)$$

High resolution transmission electron microscopy (HRTEM) images of BCN-5 and BCN-1 show the presence of 2–6 layers with an interlayer separation of approximately 3.42 Å, which is

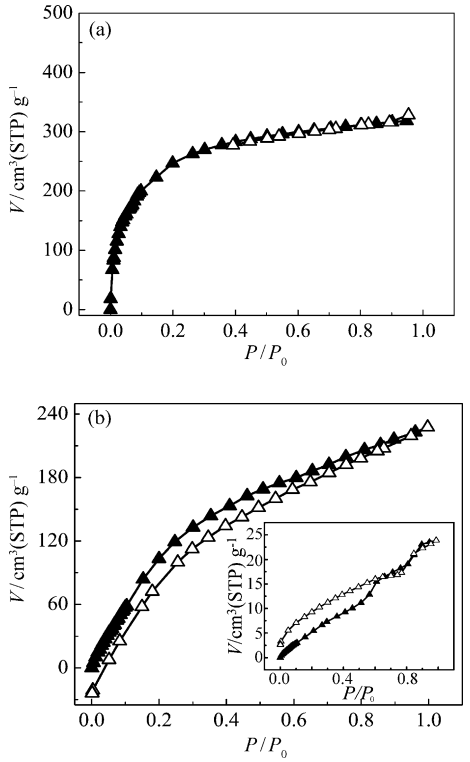

Figure 3. CO_2-adsorption (▲) and -desorption (△) isotherms at 195 K and 0.1 MPa of a) activated charcoal and b) EG; HG shown in inset.

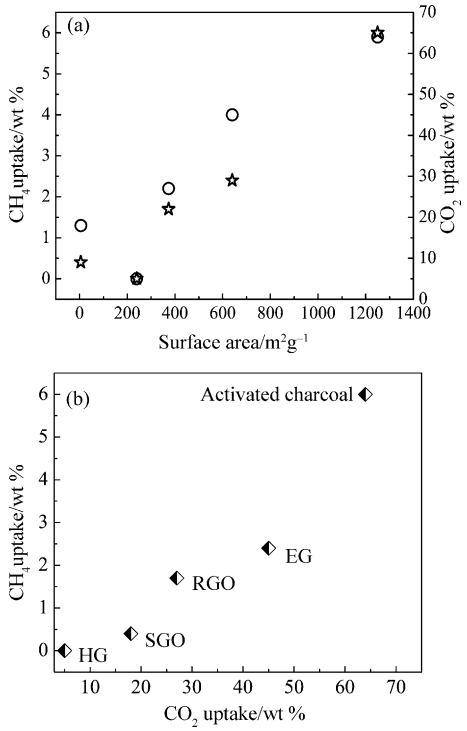

Figure 5. a) Plot of the BET surface area and the weight percentage of CH_4 uptake (☆, at 298 K and 5 MPa) and CO_2 uptake (○, at 195 K and 0.1 MPa); b) Plot of wt% of CH_4 and CO_2 uptake.

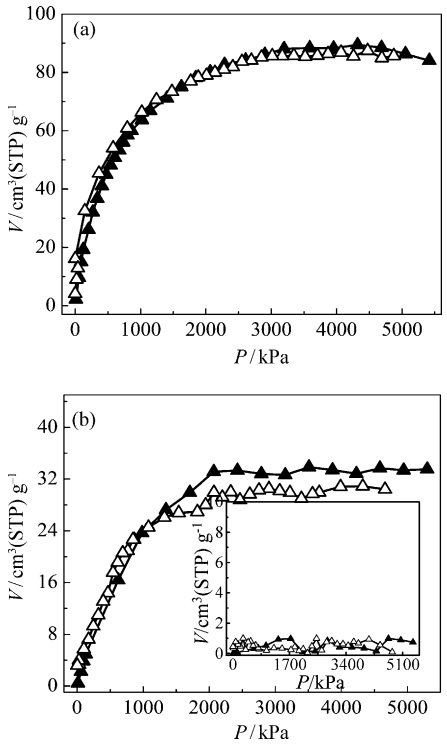

Figure 4. CH_4-adsorption (▲) and -desorption (△) isotherms at 298 K and 5 MPa of a) activated charcoal and b) EG; HG shown in inset.

higher than hexagonal BN (3.36 Å) and graphite (3.33 Å) (Figure 6a and b). Compositions of $B_xC_yN_z$ samples were examined by using X-ray photoelectron spectroscopy (XPS); typical core-level spectra of BCN-5 and BCN-1 are shown in Figure 7a and b, respectively. The 1s spectra of boron, carbon, and nitrogen are centered at 190, 284, and 399 eV, respectively.[36,42] The compositions of BCN-5 and BCN-1, estimated from the areas under the spectra by taking the capture cross sections into account, were $BC_{1.9}N$ and $BC_{1.6}N$, respectively (BC_2N for the purpose of convenience). Typical AFM images of BCN-5 and BCN-1 along with height profiles are shown in Figure 8 and reveal the presence of 2–3 layers. Our AFM investigation indicates that the majority of $B_xC_yN_z$ flakes contain 2–6 layers, as was also determined from HRTEM images. The BET surface areas of the $B_xC_yN_z$ samples were measured and typical N_2 adsorption–desorption isotherms for BCN-5 and BCN-1 at 77 K and 0.1 MPa are shown in Figure 9a and b, respectively. BCN-5 and BCN-1 gave the highest and lowest surface area values: 1990 and 1509 m^2g^{-1}, respectively. The BET surface areas of the $B_xC_yN_z$ samples are listed in Table 2.

The uptake of CO_2 by the $B_xC_yN_z$ samples were measured at 195 K and 0.1 MPa. Typical CO_2 adsorption–desorption isotherms for two $B_xC_yN_z$ samples are shown in Figure 10. The highest CO_2 uptake was observed for BCN-5, which also had the highest surface area. The CO_2 uptake for BCN-5, measured at 298 K and 5 MPa, was 64%; this uptake at room temperature is truly remarkable.

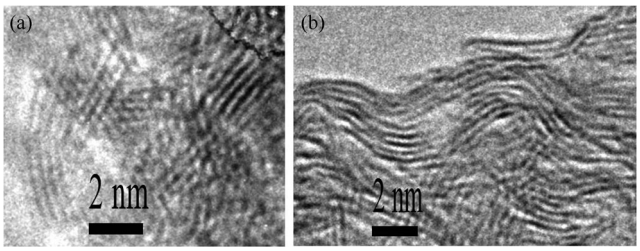

Figure 6. HRTEM images of a) BCN-5 and b) BCN-1.

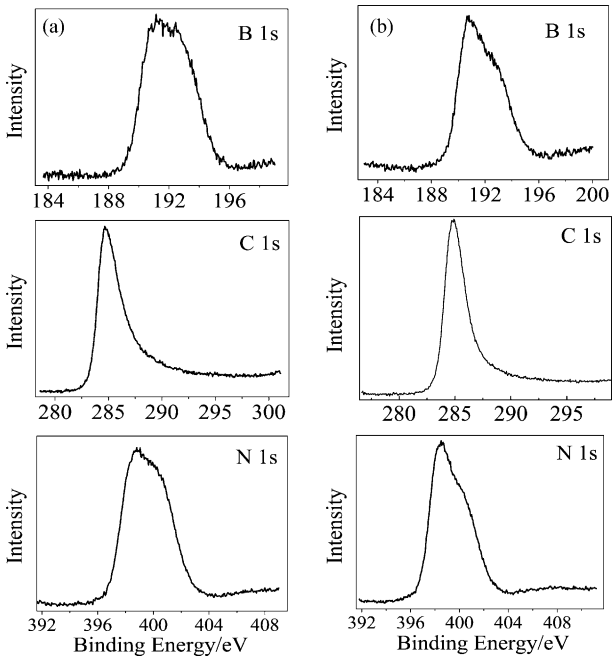

Figure 7. XPS spectra of a) BCN-5 and b) BCN-1.

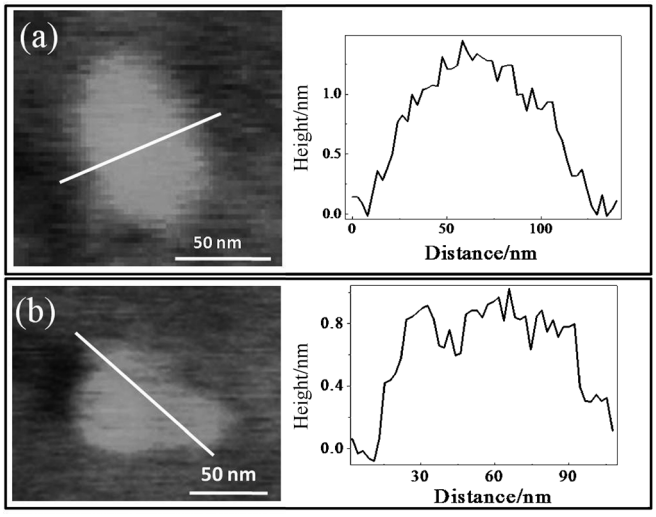

Figure 8. AFM images of a) BCN-5 and b) BCN-1 with their corresponding height profiles.

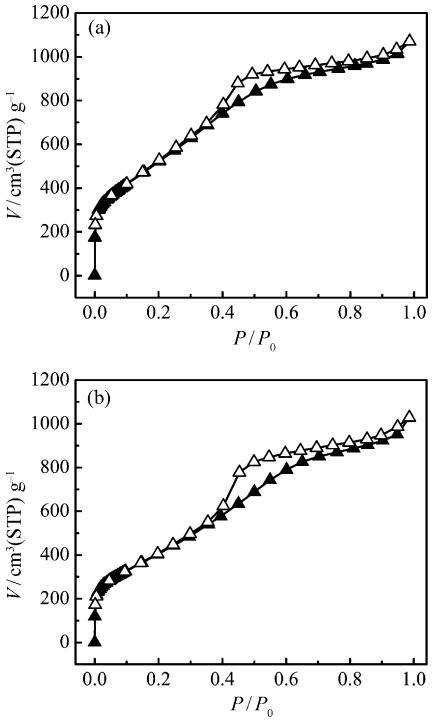

Figure 9. N_2-adsorption (▲) and -desorption (△)isotherms at 77 K and 0.1 MPa of a) BCN-5 and b) BCN-1.

Table 2. Surface area and CO_2 and CH_4 uptake for different $B_xC_yN_z$ samples.

Sample	Surface area [$m^2 g^{-1}$]	CO_2 uptake[a] [wt%]	CH_4 uptake [wt%] 273 K	298 K
BCN-1	1509	97	7.5	5.0
BCN-2	1780	100	10.5	8.4
BCN-3	1795	105	9.0	7.0
BCN-4	1853	103	10.6	9.2
BCN-5	1991	128[b]	17.3	15.0

[a] At 195 K. [b] BCN-5 shows a remarkable uptake of 64 wt% at 298 K and 5 MPa.

Typical CH_4 adsorption–desorption isotherms for BCN-5 and BCN-1 CH_4 at 298 and 273 K are given in Figure 11. The CH_4 uptake varies from 7.5 to 17% at 273 K. At 298 K, it is 5 wt% for BCN-1 and 15 wt% for BCN-5. The CH_4 uptake by BCN-5 at both temperatures is comparable with the highest CH_4 uptake values reported in literature.[28,30–32] The CH_4 uptake varies linearly with CO_2 uptake, as shown in the case of the graphene samples (Figure 12a). Figure 12b shows the variation in CO_2 and CH_4 uptake with the surface area of the $B_xC_yN_z$ samples. The uptake of both gases increases almost exponentially with the surface area. This observation may indicate that these gases have specific interactions with the high-surface-area $B_xC_yN_z$ samples, possibly because of the presence of structural entities unique to these compositions.

The experimental work presented above is complemented by first-principles calculations on the adsorption of CH_4 and CO_2 on BCN, concentrating on CH_4. Although there are known errors in density functional theory (DFT)-based estimations of

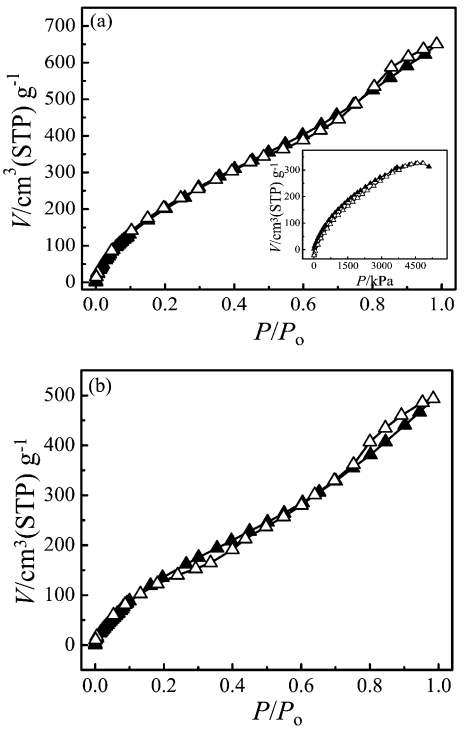

Figure 10. CO_2-adsorption (▲) and -desorption (△)isotherms at 195 K and 0.1 MPa of a) BCN-5 and b) BCN-1. The inset of (a) shows the CO_2 adsorption–desorption isotherm of BCN-5 at 298 K and 5 MPa.

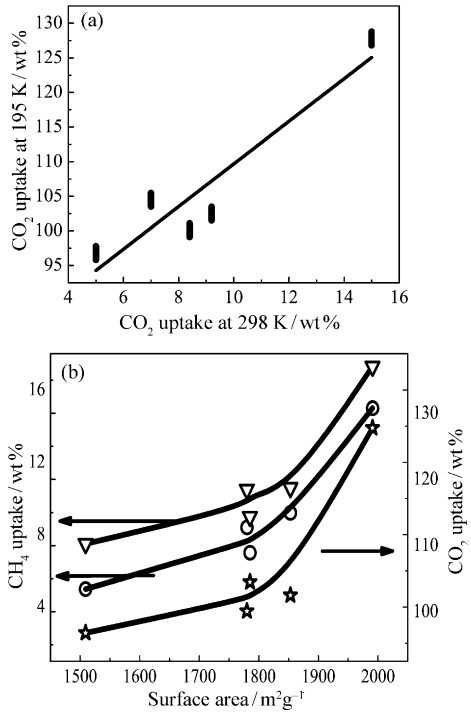

Figure 12. a) Plot of wt% uptake of CH_4 versus CO_2; b) Plot of the BET surface area versus wt% of CH_4 uptake at 5 MPa and 273 (▽) and 298 K (○) and CO_2 uptake at 0.1 MPa and 195 K (☆).

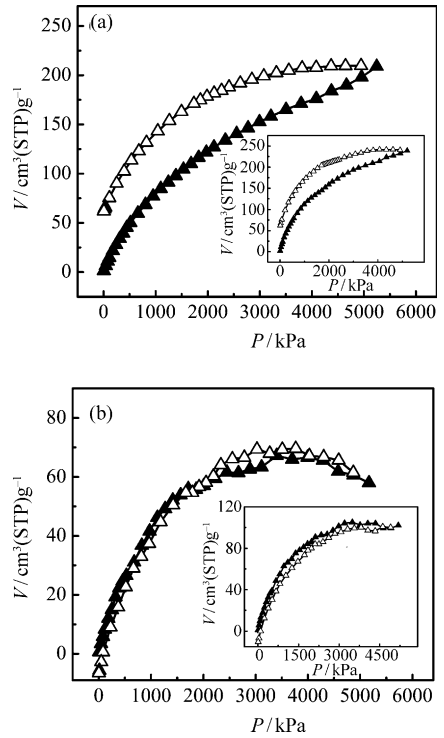

Figure 11. CH_4-adsorption (▲) and -desorption (△) isotherms at 298 K and 5 MPa of a) BCN-5 and b) BCN-1. Insets show the corresponding CH_4-adsorption–desorption isotherms at 273 K and 5 MPa.

adsorption energies attributable to neglecting van der Waals interactions, we present herein a DFT–GGA (density functional theory–generalized gradient approximation)-based analysis of the adsorption of these molecules on graphene, BN, and BCN atomic sheets, to derive trends in adsorption properties through comparison. To represent the interaction between ionic cores and valence electrons, We use the plane-wave self-consistent field (PWSCF)[43] implementation of DFT, by using a GGA[44] to exchange correlation energies of electrons and ultrasoft pseudopotentials.[45] Kohn–Sham wave functions were represented by using a plane-wave basis with an energy cutoff of 25 *Ry* and a charge-density cutoff of 150 *Ry*. BCN, BN, and graphene were simulated by using a 3X3 super cell (chosen to achieve a coverage of CH_4 comparable to coverages studied experimentally) with periodic boundary conditions and a vacuum layer of 16 Å in the direction perpendicular to atomically planar sheets. Integration over the Brillouin zone was sampled by using a Monkhorst–Pack scheme[46] with a 5X5X1 mesh of *k* points, and occupation numbers were smeared by using the Methfessel–Paxton scheme[47] with broadening of 0.03 *Ry*. This methodology was applied successfully previously.[36] In the case of CH_4 adsorption, CH_4 molecules with different orientations were placed at various possible sites in the initial configuration, and the structure was relaxed to minimize its energy. For BCN, we considered various configurations of chemical ordering of B and N atoms on graphene, and used the lowest energy configuration in the analysis of CH_4 adsorption.

The structure (both atomic positions and the periodicity of the supercell) was relaxed to a minimum energy for six differ-

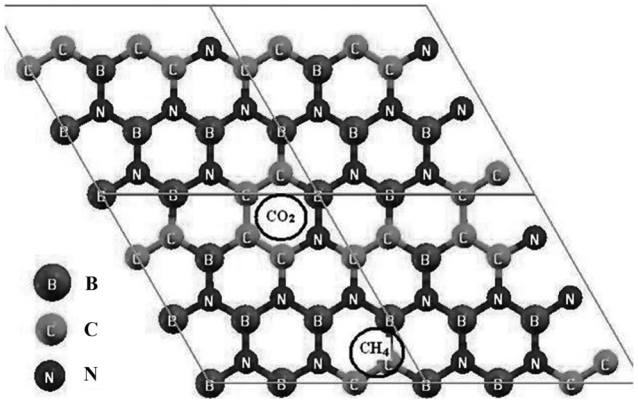

Figure 13. Preferred sites of CH_4 and CO_2 adsorption on BCN.

ent cases of chemical ordering, and the optimized structure is shown in Figure 13. The lattice constant of these configurations varies within 1% of each other and is the smallest (7.52 Å) for the lowest-energy configuration. Substitution of B and N atoms for 2/3 of the C atoms results in an expansion of the graphene lattice by approximately 1.5–2%. In the structure, there are interlinked local structural motifs of BN_3 and NB_3.

In the case of CH_4 adsorption, we placed these molecules in the supercell with 3×3 unit cells (18 atoms) with different coverages near the BCN, BN, and graphene sheets, corresponding to 7, 13, and 18 wt% adsorption respectively. In each case, we considered various sites of adsorption of CH_4: a) above atoms (B, C, and N), b) centre of a hexagonal ring (pore), and c) bond centers. In each case, the structure is relaxed by keeping the periodicity fixed, and the adsorption energy E_{ads} is determined by using Equation (5):

$$E_{ads}^{CH4/BCN} = [E_{m-CH4/BCN} - (E_{BCN} + m \times E_{CH4})]/m \quad (5)$$

in which m is the number of CH_4 molecules, E_{BCN}, E_{CH4} and $E_{m-CH4/BCN}$ are the energies of the optimized structures of BCN, an isolated CH_4 molecule, and a supercell with CH_4 on a BCN layer, respectively. A similar procedure is used in the investigation of the adsorption of CH_4 on graphene and BN.

We first study the interaction between CH_4 and BCN from studies of adsorption at the lowest coverage (7 wt%, one CH_4 molecule per supercell), where the effects of the interactions between a CH_4 molecule and its images are weak. The following atomic sites in BCN are found to be strongly adsorbing sites: a) a B atom bonded with at least one C atom, which is likely to be a weakly negative ion, b) a hexagonal ring consisting of at least two C atoms along with B and N atoms, and c) a C atom bonded with two B atoms, which would develop a slightly negative charge to attract the molecule. Adsorption of CH_4 at the boron–carbon bond is found to be stronger than at the atomic or pore sites (Figure 13).

The lowest-energy configuration (i.e., energy of adsorption of CH_4 with 7 wt% on BCN) is $-2.08\ kJ\,mol^{-1}$, which is higher than for graphene ($-1.97\ kJ\,mol^{-1}$). At a higher coverage of 13 wt% (two CH_4 molecules per supercell), the interactions between nearby CH_4 molecules become important. Our estimate of adsorption energy at this coverage on BCN is $-2.72\ kJ\,mol^{-1}$, compared to $-2.27\ kJ\,mol^{-1}$ on graphene. At a coverage of 18 wt% (three CH_4 molecules per supercell), we find the strongest binding with an adsorption energy of $-2.96\ kJ\,mol^{-1}$ on BCN, which is almost the same as on graphene. For an even higher coverage of 24 wt% (four CH_4 molecules per supercell), we find that adsorption is not energetically favorable (Figure 14). This is largely attributable to interactions between CH_4 molecules at small separations of the layers. Thus, we find that adsorption is stronger than on graphene for all coverages of CH_4 on BCN. Typically, the distance between the adsorbed CH_4 molecule and the BCN plane is approximately 3% smaller than that between the CH_4 molecule and graphene, reflecting a stronger bonding with the lattice. The optimized structures for the adsorption of three methane molecules on BCN and graphene are shown in Figure 15a and b, respectively.

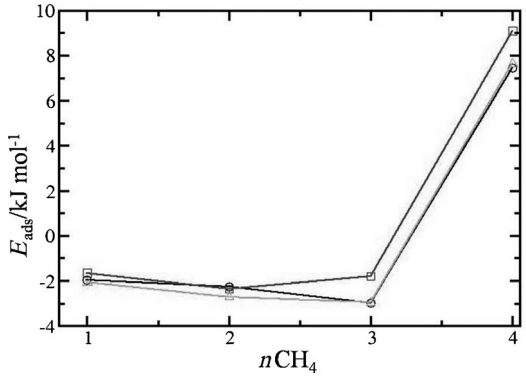

Figure 14. Coverage-dependent adsorption energies of CH_4 on graphene (○), BN (□), and BCN (△).

The adsorption energies can be broken up as shown in Equation (6):

$$E = E_1 - E_2 = [E_{n,m} - E_n - m \times E_{CH4}] - [E_{mCH4} - m \times E_{CH4}] \quad (6)$$

in which E_1 is the total absorption energy and E_2 is the CH_4–CH_4 interaction energy, so E gives a measure of the adsorption energy after removing the CH_4–CH_4 interaction energy whereas $E_{n,m}$ is the energy of a complex with m methane molecules in a supercell with n atoms, E_n the energy of BCN, BN, or graphene, and E_{CH4} the energy of one CH_4 molecule in the same supercell. In our calculations, we found that CH_4–CH_4 interactions play an important role (Table 3), which is taken into consideration by the difference $E_1 - E_2$.

Methane adsorbed on graphene, BN, and BCN develops a small electric dipole moment at low coverages on graphene, BN, and BCN. The dipole moments is strongest when CH_4 is adsorbed on BCN, when mainly electrostatic interactions are relevant. Obviously, the energy E is similar for graphene and BCN for any amount of methane adsorption (i.e., for a given surface

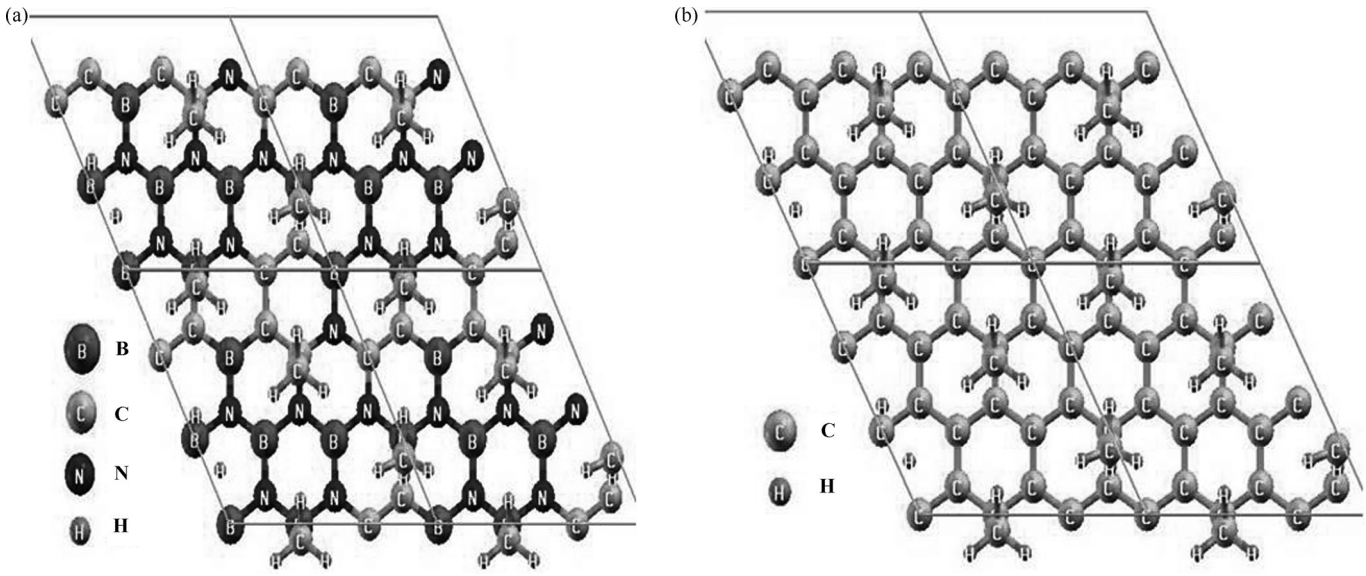

Figure 15. Structure and sites of CH_4 adsorption at optimal (ca. 18 wt%) coverage on a) BCN and b) graphene.

Table 3. Energies of CH_4 adsorption on graphene, BN, and BCN.

Sample	*n*	*m*	E_1 [kJ mol^{-1}]	E_2 [kJ mol^{-1}]	E_1-E_2 [kJ mol^{-1}]
Graphene	18	1	−1.97	0.00	−1.97
		2	−2.27	−1.41	−0.86
		3	−2.97	−2.05	−0.92
BN	18	1	−1.66	0.00	−1.66
		2	−2.35	−1.41	−0.94
		3	−1.80	−2.05	0.25
BCN	18	1	−2.08	0.00	−2.08
		2	−2.72	−1.41	−1.31
		3	−2.96	−2.05	−0.91

area, the methane adsorption on graphene and BCN is almost similar). From Figures 5a and 12b, it can be deducted that methane uptake is quite similar for graphene and BCN having the same surface area (1300 $m^2 g^{-1}$), which supports the results obtained from theoretical calculation. Our results also establish the optimal loading on BCN to store methane as 18 wt%.

CO_2 adsorption occurs strongly at the following atomic sites in BCN:[36] a) a N atom bonded with at least one C atom, which is likely to be a weakly negative ion, b) a B atom bonded with one N atom and one C atom, which would attract the negatively charged O atom of the molecule, and c) a hexagonal ring consisting of four C atoms and one B and one N atom (Figure 13).

We estimate an adsorption energy of −2.79 and approximately 3.67 kJ mol^{-1} at 20 and 40 wt% coverage of CO_2 on BCN, respectively. On graphene, the adsorption energy is −1 kJ mol^{-1} at 40 wt% coverage. At 60 wt% coverage, the adsorption energy is −3.73 kJ mol^{-1} on BCN compared to −2.04 kJ mol^{-1} for graphene. Furthermore, the distance between the CO_2 molecules and the BCN plane is shorter by 3% than in the case of graphene. The distance between the CO_2 molecule and the BCN plane at 40 and 60 wt% coverage are 3.74 and 3.89 Å, respectively.

Comparing our results with those from the theoretical studies performed by Thierfelder et al.[48] on the adsorption of CH_4 on graphene, our estimates of adsorption energies are somewhat underestimated because van der Waals interactions are neglected. Our results are, however, in good agreement with the GGA-based estimates of Thierfelder et al., and we expect that the binding energy between CH_4 and BCN to be stronger by approximately 8 kJ mol^{-1} than is suggested by our calculations. Our goal in the present study is to determine the trend in adsorption energies with coverage and the optimum coverage of adsorption. Our calculations by using DFT-GGA are useful in understanding the experimental results.

We have performed preliminary calculations on the interaction of CO_2 and CH_4 with BC_2N after obtaining its optimized structure. Again, both CH_4 and CO_2 interact more strongly with BC_2N than with graphene. It appears that BC_2N is even better than BCN as an adsorbent for these gases.

Conclusions

The present study clearly shows that graphene samples exhibit reasonable uptake values of CO_2, but low uptake values for CH_4. The uptake values of CO_2 and CH_4 by graphene are both considerably lower than those by activated carbon. The uptake values of CO_2 and CH_4 vary linearly with the surface area of the samples. Graphene-like $B_xC_yN_z$ samples, on the other hand, have large surface areas and a very high uptake of both CO_2 and CH_4. These uptake values increase exponentially with the surface area of the $B_xC_yN_z$ samples. In general, the uptake of CH_4 varies linearly with that of CO_2. The experimental results, along with our theoretical calculations, reveal that the high uptake of CO_2 and CH_4 by the BCN samples could arise from the larger surface area, probably related to the weaker rippling strength compared to graphene and the presence of fewer defects. Our calculations also simulate the experimental uptake values satisfactorily.

Experimental Section

We prepared four few-layer graphene samples designated EG, HG, RGO, and SGO. The sample EG was prepared by thermal exfoliation of graphite oxide (GO) at high temperatures.[37–39] In this procedure, GO (0.2 g) was placed in an alumina boat and inserted into a long quartz tube sealed at one end. The sample was purged with Ar for 10 min, and then the quartz tube was quickly inserted into a tube furnace preheated to 1050 °C and held in the furnace for 10 min. HG was prepared by arc evaporation of graphite in the presence of hydrogen without a catalyst.[40] In this process, direct-current arc discharge of graphite evaporation was performed in a water-cooled stainless steel chamber filled with a mixture of hydrogen (2.7×10^4 Pa) and helium (6.7×10^4 Pa). In a typical experiment, a graphite rod (Alfa Aesar with 99.999% purity; 6 mm in diameter and 50 mm long) was used as the anode and a second graphite rod (13 mm in diameter and 60 mm in length) was used as the cathode. The discharge current was in the range of 100–150 A, with a maximum open circuit voltage of 60 V. To prepare RGO, single-layer graphene oxide (SGO) obtained by ultrasonication of GO was reacted with hydrazine hydrate under refluxing.[41] In this method, hydrazine hydrate (1 mL) was added to a stable aqueous SGO solution (100 mL, 1 mg 1 mL^{-1}) and heated under reflux for 24 h. Reduced SGO turns black and precipitates at the bottom of the flask. The resulting precipitate was filtered and washed with water and methanol.

$B_xC_yN_z$ samples were prepared by the high temperature reaction of boric acid and urea with high-surface-area activated charcoal (1250 m^2g^{-1}).[36] The ratio of boric acid to urea was varied between 1:6 and 1:24 while keeping the amount of activated charcoal fixed (0.5 g). For BCN-1, BCN-4, and BCN-5 the molar ratio of boric acid to urea was 1:24 (0.1 g H_3BO_3 and 2.4 g urea), whereas the ratio was 1:12 and 1:6 for BCN-2 and BCN-3, respectively. The aqueous mixture of H_3BO_3, urea, and activated carbon was sonicated for 30 min, followed by evaporation of water at 70 °C, to give a viscous slurry. The slurry was transferred to a quartz boat and heated under N_2 flow. To obtain BCN-1 and BCN-2 samples, the mixture was heated at 900 °C for 18 h. To obtain BCN-3, BCN-4, and BCN-5, the mixture was heated at 950, 1000, and 900 °C, respectively, for 12 h. The products were cooled to room temperature and subsequently heated in an ammonia atmosphere at 930 °C for 3 h to obtain black $B_xC_yN_z$. These samples were subjected to elemental analysis and other characterization techniques.

The morphology of the samples was examined by using a TEM with a Tecnai T20 instrument (FEI) operated at an accelerating voltage of 200 kV. AFM measurements were performed by using an Innova atomic force microscope in the tapping mode. X-ray photoelectron spectroscopy (XPS) measurements were performed by using an Omicron spectrometer employing AlK_α radiation (1486.6 eV). Raman spectra were recorded by employing a LabRAM HR with a $\lambda = 633$ nm line from a HeNe laser. FTIR spectra were recorded by using a Bruker IFS 66v/S spectrometer. Powder XRD patterns of the products were recorded by using a Bruker-D8 X-ray diffractometer using CuK_α radiation. Nitrogen adsorption (surface area) measurements and CO_2 uptake experiments were performed in a Quanta Chrome Autosorb-1 instrument. CH_4-uptake experiments were carried out by using a BELSORP-aqua3 analyzer.

Keywords: adsorption · borocarbonitrides · carbon dioxide fixation · density functional calculations · graphene

[1] K. M. K. Yu, I. Curcic, J. Gabriel, S. C. E. Tsang, *ChemSusChem* **2008**, *1*, 893 – 899.
[2] D. W. Keith, *Science* **2009**, *325*, 1654 – 1655.
[3] A. Wahby, J. M. Ramos-Fernández, M. Martínez-Escandell, A. Sepúlveda-Escribano, J. Silvestre-Alberto, F. Rodríguez-Reinoso, *ChemSusChem* **2010**, *3*, 974 – 981.
[4] S. A. Freeman, R. Dugas, D. Van Wagener, T. Nguyen, G. Rochelle, *Energy Procedia* **2009**, *1*, 1489 – 1496.
[5] S. Zhou, X. Chen, T. Nguyen, A. K. Voice, G. T. Rochelle, *ChemSusChem* **2010**, *3*, 913 – 918.
[6] A. Jensen, R. Christensen, *Acta Chem. Scand.* **1955**, *9*, 486 – 492.
[7] O. Trass, R. H. Weiland, *Can. J. Chem. Eng.* **1971**, *49*, 773 – 781.
[8] M. M. Sharma, *Trans. Faraday Soc.* **1965**, *61*, 681 – 688.
[9] E. Sada, H. Kumazawa, M. A. Butt, *Chem. Eng. J.* **1977**, *13*, 213 – 217.
[10] H. Hikita, S, Asai, H. Ishikawa, M. Honda, *Chem. Eng. J.* **1977**, *13*, 7 – 12.
[11] J. Li, A. Henni, P. Tontiwachwuthikul, *Ind. Eng. Chem. Res.* **2007**, *46*, 4426 – 4434.
[12] J. Zhang, B. Han, Y. Zhao, J. Li, M. Hou, G. Yang, *Chem. Commun.* **2011**, *47*, 1033 – 1035.
[13] R. J. Perry, T. A. Grocela-Roach, M. J. O'Brien, S. Genovese, B. R. Wood, L. N. Lewis, H. Lam, G. Soloveichik, M. Rubinsztajn, S. Draper, R. M. Enick, J. K. Johnson, H.-b. Xie, D. Tapriyal, *ChemSusChem* **2010**, *3*, 919 – 930.
[14] K. Simons, K. Nijmeijer, H. Mengers, W. Brilman, M. Wessling, *ChemSusChem* **2010**, *3*, 939 – 947.
[15] S. Chakravarti, A. Gupta, B. Hunek, *Advanced Technology for the Capture of Carbon Dioxide from Flue Gases*, First National Conference on Carbon Sequestration, Washington DC, **2001**.
[16] A. O. Yazaydin, R. Q. Snurr, T. H. Park, K. Koh, J. Liu, M. D. LeVan, A. I. Benin, P. Jakubczak, M. Lanuza, D. B. Galloway, J. J. Low, R. R. Willis, *J. Am. Chem. Soc.* **2009**, *131*, 18 198 – 18 199.
[17] Y. S. Bae, O. K. Farha, J. T. Hupp, R. Q. Snurr, *J. Mater. Chem.* **2009**, *19*, 2131 – 2134.
[18] A. O. Yazaydin, A. I. Benin, S. A. Faheem, P. Jakubczak, J. J. Low, J. J. Low, R. Q. Snurr, *Chem. Mater.* **2009**, *21*, 1425 – 1430.
[19] Y. S. Bae, O. K. Farha, A. M. Spokoyny, C. A. Mirkin, J. T. Hupp, R. Q. Snurr, *Chem. Commun.* **2008**, 4135 – 4137.
[20] R. V. Siriwardane, M. S. Shen, E. P. Fisher, J. A. Poston, *Energy Fuels* **2001**, *15*, 279 – 284.
[21] Y. Belmabkhout, A. Sayari, *Chem. Eng. Sci.* **2009**, *64*, 3729 – 3735.
[22] S. Himeno, T. Komatsu, S. Fujita, *Adsorption* **2005**, *11*, 899 – 904.
[23] A. Kapoor, R. T. Yang, *Chem. Eng. Sci.* **1989**, *44*, 1723 – 1733.
[24] B. D. Freeman, *Macromolecules* **1999**, *32*, 375 – 380.
[25] R. W. Baker, *Ind. Eng. Chem. Res.* **2002**, *41*, 1393 – 1411.
[26] V. Goetz, O. Pupier, A. Guillot, *Adsorption* **2006**, *12*, 55 – 63.
[27] W. R. Alesi, M. Gray, J. R. Kitchin, *ChemSusChem* **2010**, *3*, 948 – 956.
[28] M. Eddaoudi, J. Kim, N. Rosi, D. Vodak, J. Wachter, M. O'Keeffe, O. M. Yaghi, *Science* **2002**, *295*, 469 – 472.
[29] A. C. Sudik, A. R. Millward, N. W. Ockwig, A. P. Côté, J. Kim, O. M. Yaghi, *J. Am. Chem. Soc.* **2005**, *127*, 7110 – 7118.
[30] S. Ma, D. Sun, J. M. Simmons, C. D. Collier, D. Yuan, H. C. Zhou, *J. Am. Chem. Soc.* **2008**, *130*, 1012 – 1016.
[31] H. Wu, W. Zhou, T. Yildirim, *J. Am. Chem. Soc.* **2009**, *131*, 4995 – 5000.
[32] H. Wu, J. M. Simmons, Y. Liu, C. M. Brown, X. S. Wang, S. Ma, V. K. Peterson, P. D. Southon, C. J. Kepert, H. C. Zhou, T. Yildirim, W. Zhou, *Chem. Eur. J.* **2010**, *16*, 5205 – 5214.
[33] J. Lan, D. Cao, W. Wang, *Langmuir* **2010**, *26*, 220 – 226.
[34] H. Wu, W. Zhou, T. Yildirim, *J. Phys. Chem. C* **2009**, *113*, 3029 – 3035.
[35] D. Lozano-Castelló, J. Alcañiz-Mongea, M. A. de la Casa-Lillo, D. Cazorla-Amorós, A. Linares-Solano, *Fuel* **2002**, *81*, 1777 – 1803.
[36] K. Raidongia, A. Nag, K. P. S. S. Hembram, U. V. Waghmare, R. Datta, C. N. R. Rao, *Chem. Eur. J.* **2010**, *16*, 149 – 157.
[37] a) W. Hummers, R. E. Offeman, *J. Am. Chem. Soc.* **1958**, *80*, 1339; b) L. Staudenmaier, *Ber. Dtsch. Chem. Ges.* **1898**, *31*, 1481 – 1487.
[38] H. C. Schniepp, J. L. Li, M. J. McAllister, H. Sai, M. Herrera-Alonso, D. H. Adamson, R. K. Prud'homme, R. Car, D. A. Saville, I. A. Aksay, *J. Phys. Chem. B* **2006**, *110*, 8535 – 8539.
[39] K. S. Subrahmanyam, S. R. C. Vivekchand, A. Govindaraj, C. N. R. Rao, *J. Mater. Chem.* **2008**, *18*, 1517 – 1523.
[40] K. S. Subrahmanyam, L. S. Panchakarla, A. Govindaraj, C. N. R. Rao, *J. Phys. Chem. C* **2009**, *113*, 4257 – 4259.
[41] S. Stankovich, D. A. Dikin, R. D. Piner, K. A. Kohlhaas, A. Kleinhammes, Y. Jia, Y. Wu, S. T. Nguyen, R. S. Ruoff, *Carbon* **2007**, *45*, 1558 – 1565.

[42] S. Y. Kim, J. Park, H. C. Choi, J. P. Ahn, J. Q. Hou, H. S. Kang, *J. Am. Chem. Soc.* **2007**, *129*, 1705 – 1716.
[43] Code used for first-principles calculations in this work: S. Baroni, A. Dal Corso, S. de Gironcoli, P. Gianozzi, http://www.pwscf.org (accessed August 2011).
[44] J. P. Perdew, K. Burke, M. Ernzerhof, *Phys. Rev. Lett.* **1996**, *77*, 3865 – 3868.
[45] D. Vanderbilt, *Phys. Rev. B.* **1990**, *41*, 7892 – 7895.
[46] H. J. Monkhorst, J. D. Pack, *Phys. Rev. B.* **1976**, *13*, 5188 – 5192.
[47] M. Methfessel, A. Paxton, *Phys. Rev. B.* **1989**, *40*, 3616 – 3621.
[48] C. Thierfelder, M. Witte, S. Blankenburg, E. Rauls, W. G. Schmidt, *Surf. Sci.* **2011**, *605*, 746 – 749.

Received: April 18, 2011
Published online on August 25, 2011

